

α -RuCl₃ intercalated into graphite: a new three-dimensional platform for exotic quantum phases

Aleksandar Razpopov,^{1,*} Shirin Mozaffari,^{2,3,†} Takahiro Matsuoka,^{2,4,‡}
Matthew Cothrine,² Nan Huang,² Roser Valentí,^{1,§} and David Mandrus^{2,¶}

¹*Institut für Theoretische Physik, Goethe-Universität, 60438 Frankfurt am Main, Germany*

²*Department of Materials Sciences and Engineering,
The University of Tennessee, Knoxville, TN 37996, USA*

³*Department of Physics and Astronomy, Clemson University, Clemson, SC 29634, USA*

⁴*National Institute of Physics, University of the Philippines Diliman, Quezon, Metro Manila 1101, Philippines*

(Dated: February 3, 2026)

Multilayer graphene with different stacking sequences has emerged as a powerful setting for correlated and topological phases. In parallel, progress in graphene heterostructures with magnetic or correlated materials—most notably the Kitaev candidate α -RuCl₃—has demonstrated charge transfer, magnetic proximity effects, and interfacial reconstruction, creating new opportunities for engineered quantum systems. Motivated by these developments, we explore a three-dimensional analogue in which α -RuCl₃ layers are inserted directly into the van der Waals gaps of graphite, forming an intercalated system. Here, we report the successful synthesis and comprehensive characterization of graphite intercalated with α -RuCl₃. Using a combination of X-ray diffraction, quantum oscillation measurements, and first-principles electronic structure calculations, we study the structural and electronic properties of this intercalated crystals. Our results demonstrate that graphite intercalated with α -RuCl₃ offers a robust route to develop three-dimensional materials with access to novel correlated and topological states.

INTRODUCTION

In recent years, multilayer Bernal-stacked graphene (AB) and graphene with rhombohedral (ABC) stacking have emerged as remarkable platforms for correlated and topological quantum phenomena [1–6]. In particular, experimental studies of rhombohedral graphene have revealed the formation of flat-band states, interaction-driven insulating phases, magnetism, and superconductivity in devices with just a few stacked layers. For example, in tetralayer or higher ABC-stacked graphene the interplay of low-density carriers, large Berry curvature, and strong Coulomb interactions has given rise to anomalous Hall and superconducting states [7–9]. These advances underscore the power of stacking geometry, interlayer coupling, and band flattening to access exotic electronic ground states in a purely carbon-based van der Waals system.

At the same time, heterostructures coupling graphene with two-dimensional magnetic or correlated materials are rapidly expanding the playground of quantum phenomena. One prominent example is the van der Waals assembly of graphene with α -RuCl₃ [10–14], a layered Mott insulating Kitaev material candidate [15–18]. In these α -RuCl₃/graphene heterostructures, transport experiments provide evidence for both charge transfer and magnetic proximity effects [10, 11, 13], while theoretical studies point to

strain, enhanced Kitaev interactions, and interface-driven electronic reconstruction [12, 13]. The observation of nanometer-scale p–n junctions in STM measurements [19] further illustrates the richness of the interfacial physics in these systems [20].

In this work, we report the successful growth and characterization of graphite intercalated with α -RuCl₃. By combining synthesis, X-ray measurements, quantum oscillation studies, and first-principles electronic structure calculations, we fully characterize the samples and introduce with them a new class of three-dimensional crystals.

These findings open pathways to engineer interfaces that combine flat-band physics, magnetism, and proximity effects, following a long tradition of magnetically intercalated graphite [21, 22]. Bringing these threads together, the prospect of graphite intercalated with α -RuCl₃ (i.e., inserting layers of α -RuCl₃ into the van der Waals gaps of graphite or few-layer graphene) is particularly compelling. On the one hand, the flat-band and correlation physics of rhombohedral graphene suggest that modifier layers – such as intercalants – can tune the carrier density, screening, and interlayer coupling in ways that may enhance or stabilize exotic phases. On the other hand, the graphene/ α -RuCl₃ heterostructure results show that α -RuCl₃ is a highly effective electron acceptor and magnetically active component with possible spin-liquid behavior in close proximity to graphene sheets. Intercalating α -RuCl₃ into graphite therefore provides a pathway to realizing a three-dimensional analogue of these phenomena, as illustrated in Figure 1.

* razpopov@itp.uni-frankfurt.de

† shirinm@clemson.edu

‡ tmatsuoka@up.edu.ph

§ valenti@itp.uni-frankfurt.de

¶ dmandrus@utk.edu

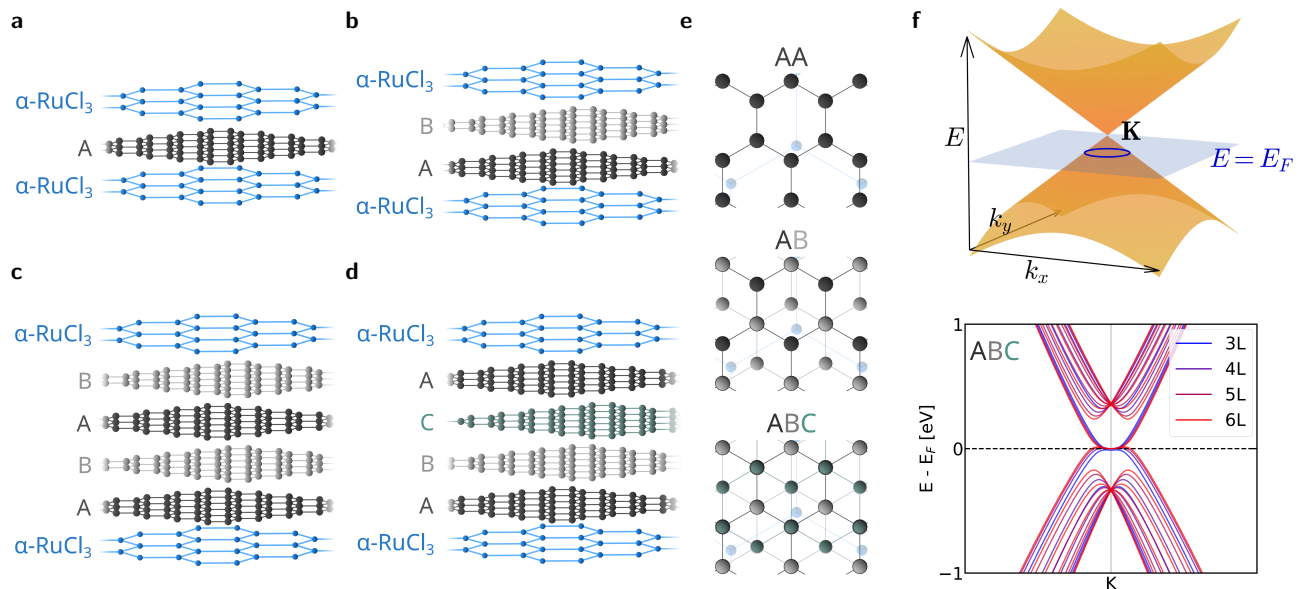


Figure 1. Different intercalation stackings: **a** A|A, **b** AB|AB (stage 2: S2), **c** ABAB|ABAB (stage 4: S4), and **d** ABCA|ABCA (stage 4: S4). **e** Stacking top view. The α -RuCl₃ layer is denoted by a blue layer, while the labels A,B, and C denote the different graphene stackings. **f** The upper panel illustrates charge transfer effects due to proximity of α -RuCl₃ to graphene. The lower panel depicts the evolution of the band structure in ABC-stacked graphene.

RESULTS AND DISCUSSION

Synthesis

The synthesis of graphite intercalates can be performed using an intercalate in the vapor, liquid, or solid phase. Fabrication methods include solid-state, molten salt, two-zone vapor transport intercalation, and hydrothermal synthesis [21, 23–27]. Among these, two-zone vapor transport is most widely used to intercalate volatile material into the graphite. We grew the intercalated graphite samples via a chemical vapor transport (CVT) method. Three starting constituents were sealed in a quartz ampule: 1) single crystals of graphite, in the form of natural graphite flakes from HQ graphene (99.98% purity), 2) pure α -RuCl₃ powder from Furuya Metals, and 3) AgCl powder from Sigma Aldrich (99.998% purity). The weight ratio used to synthesize intercalated graphite was C : α -RuCl₃ : AgCl 0.03g : 0.2g : 0.5g. The α -RuCl₃ powder was pressed into a pellet to keep it together, and the AgCl powder was initially kept in an alumina crucible. We found that without excess Cl₂, α -RuCl₃ would not intercalate into graphite. To generate a Cl₂-rich atmosphere, Cl₂ gas was generated by shining UV light on the AgCl powder until it decomposed, leaving behind Ag powder. We used powdered AgCl to increase the surface area exposed to UV light. Typically, the sample was irradiated with UV light for 3–5 minutes, until most of the powder turned dark brown. The AgCl section of the tube was then sealed off, leaving the graphite flakes, α -RuCl₃ pellet, and an enhanced Cl₂ atmosphere. This is schematically shown in Figure 2a. After the ampule was prepared, synthesis was carried out in a two-zone tube fur-

nace. The graphite end was placed in the high temperature zone, which was held at 900 °C, while the α -RuCl₃ end was held at 830 °C. After 22 hours, stage 4 α -RuCl₃ intercalated into graphite, that we denote C-RuCl₃ was formed. Continuing the reaction for a total of 48 hours resulted in stage 2 C-RuCl₃. Continuing the reaction further led to mixed stage intercalation and/or disordered compounds.

Structure analysis

By utilizing the structural analogy to other transition metal trichlorides, different intercalation stackings shown in Figure 1 are anticipated for α -RuCl₃-intercalated graphite [28–30]. In Figure 1, A, B and C denote different orientations of the graphene layers and “|” represents one α -RuCl₃ layer. X-ray diffraction (XRD) experiments of powdered samples resulted in two values for the c-axis and both of them show a significant expansion with respect to the c-axis of graphite (6.7 Å → 25.4(2) Å and 58.2(1) Å), suggesting the successful intercalation of α -RuCl₃ between the layers (see Figures S1a and b in the supplemental material). From the structural analogy to other transition metal-trichlorides, we concluded the synthesized samples are stage 2 (S2) and stage 4 (S4) samples (Figure 1b, c, and d). In the S2 sample, two graphene layers are sandwiched by two α -RuCl₃ layers, while in S4, four graphene layers are sandwiched by two α -RuCl₃ layers. XRD spots from single crystal (highly oriented polycrystalline) S2 and S4 samples can be indexed with hexagonal structures, with a small portion of residual pure graphite (see Figures S1b and c in the supplemental material). The estimated a-axes are 29.62(3) Å for S2

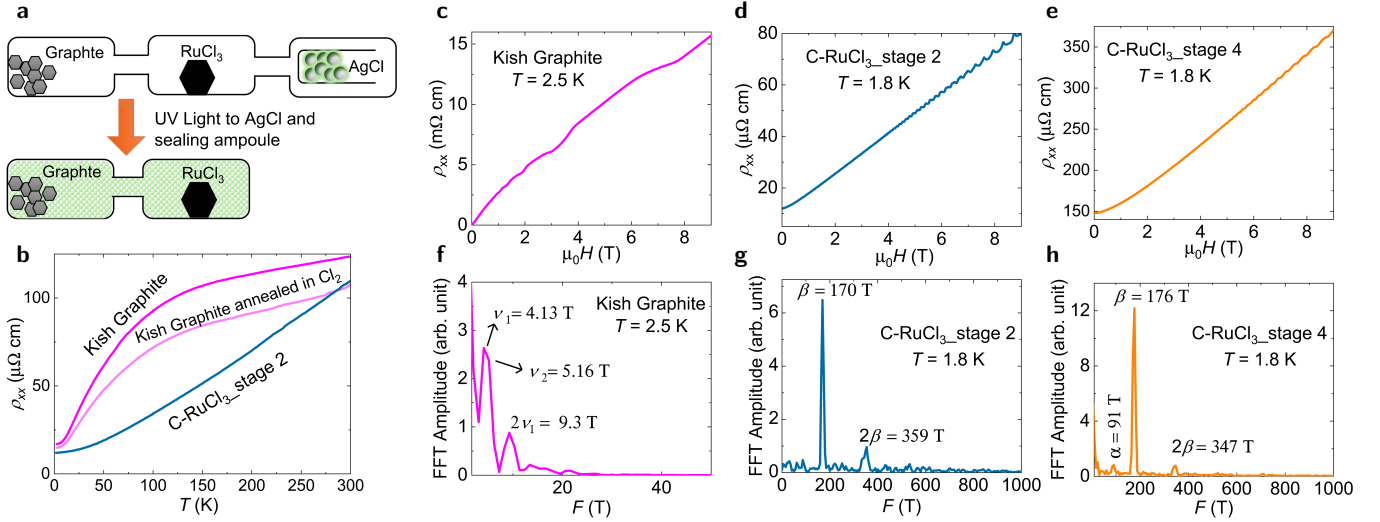


Figure 2. **a** Schematic of two-zone vapor transport using AgCl as a chlorine source to grow C-RuCl₃ samples. **b** Temperature dependence of the longitudinal resistivity of Kish graphite as received and after annealing in Cl₂ gas, and C-RuCl₃ stage 2 sample. **c**, **d**, and **e** Magnetic field dependence of the longitudinal resistivity ρ_{xx} of Kish graphite, C-RuCl₃ stage 2, and C-RuCl₃ stage 4 samples, respectively. **f**, **g**, and **h** Fast Fourier transform (FFT) of the oscillatory component of resistivity shown in **c**, **d**, and **e** for $\mu_0 H$ applied out-of-plane. Peaks correspond to the extremal cross-sectional areas of the Fermi surface and are labeled as ν for Kish graphite, α and β for the intercalated samples.

and 29.5(A) Å for S4. The $N_1 \times M_1 \times 1$ graphene and $N_2 \times M_2 \times 1$ α -RuCl₃ unit cells alternate in the crystallographic c -direction forming super lattices in both samples, where N_1 , N_2 , M_1 , M_2 are integers.

The obtained lattice constants and stackings are summarized in Table I and Figure 1. For the details of experimental setups and the structure analysis, see the Methods section and the Supplementary materials.

Transport and Shubnikov-de Haas quantum oscillations

Figure 2b shows the temperature dependence of the longitudinal resistivity for three samples: pristine Kish graphite, Kish graphite annealed in Cl₂ gas, and graphite intercalated with α -RuCl₃, denoted C-RuCl₃. Pristine Kish graphite was used as a reference. To isolate the effects of the synthesis procedure, we also annealed graphite in a chlorine atmosphere at 900 °C for several days in a sealed tube without a α -RuCl₃ pellet ensuring any observed changes were not solely due to the annealing environment. It is important to note that the reported resistivity values should not be considered absolute, as the samples are flaky and irregular in shape. While we made careful efforts to estimate the sample dimensions, uncertainties remain. In particular, we found that using a blade to carve bar-shaped pieces sometimes alters the residual resistivity ratio [(RRR = R(300K)/R(2K)], likely due to mechanical damage.

Figure 2c–e present the low-temperature magnetic field dependence of the resistivity for the Kish graphite, stage 2 and stage 4 intercalated samples. For the Kish graphite, Shubnikov–de Haas (SdH) quantum oscillations are observable at

magnetic fields as low as 1.5 T. The intercalated samples exhibit SdH oscillations at $\mu_0 H > 4$ T, and with much shorter periods. The frequency of the SdH oscillations was obtained by first subtracting a smooth polynomial background from the magnetoresistivity data to isolate the oscillatory component. The oscillatory part is periodic in the inverse of the magnetic field. A Fast Fourier Transform (FFT) was then performed on the oscillatory signal to extract the oscillation frequency. The frequencies we obtained for Kish graphite are $\nu_1 = 4.13$ T and $\nu_2 = 5.16$ T, with the first harmonic of ν_1 also clearly observable; as shown in Figure 2f. This is in good agreement with previous determinations of the fundamental SdH frequencies in graphite, including those obtained using other experimental techniques [31, 32]. As shown in Figure 2g and h, the frequency of the SdH oscillations in the α -RuCl₃ intercalated graphite samples occurs around $\beta \approx 170$ –176 T. The first harmonic, shown by 2β , is also clearly observable. In addition to the main frequency, the C-RuCl₃ S4 sample shows an additional SdH oscillation frequency at $\alpha = 91$ T.

Structure optimization and charge transfer

In order to have a full characterization of the grown crystal structures and extract their electronic properties, we perform *ab initio*-based density functional theory (DFT) calculations (see Methods section). Given the considerable size of the experimental unit cells reported in Table I, carrying out calculations directly on these cells is computationally prohibitive. Therefore, we employ reduced (simplified) unit cells in which a tensile strain of $\approx 4\%$ is applied to the α -RuCl₃ layer to keep the overall cell size manageable, while

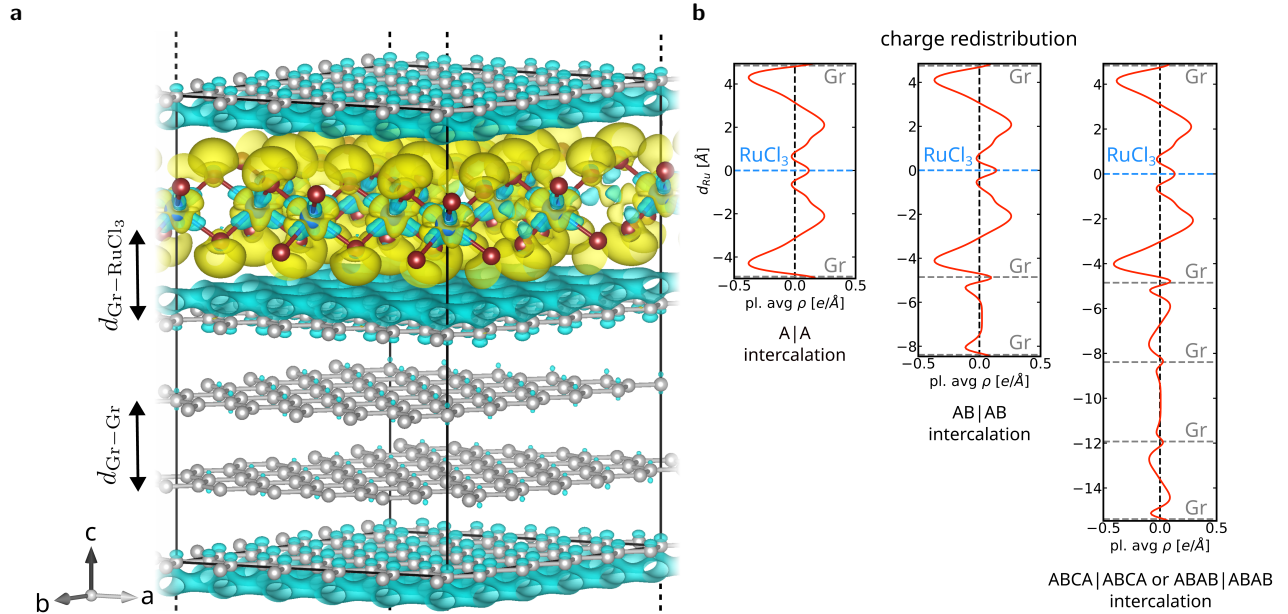


Figure 3. **a** Representative ABCA|ABCA crystal structure of C-RuCl₃ used in the DFT calculations. The blue and yellow iso-surfaces show the charge depletion and accumulation, respectively. $d_{\text{Gr-RuCl}_3}$ denotes the distance α -RuCl₃-graphene layer distance, and $d_{\text{Gr-Gr}}$ the graphene-graphene layer distance. **b** The planar-averaged charge density redistribution along the c -axis for each geometry as a function of the Ru layer distance, d_{Ru} . The reference point is the position of the Ru layer indicated by the dashed blue line, the grey dashed lines indicate the position of the graphene layers. The four-layer intercalations in the ABAB|ABAB and ABCA|ABCA stacking are represented by one plot. Crystal structure plots are generated with VESTA [33].

leaving the geometry of the graphene layers unchanged. As shown below, this simplification does not significantly affect the relevant physical observables in the transport measurements.

To verify this, we benchmark the strained structure against the unstrained one. We consider an unstrained C-RuCl₃ structure of a 5×5 α -RuCl₃ layer intercalated into a single layer of 12×12 graphene in the A|A (Figure 1a) stacking and a strained unit cell consisting of a 2×2 α -RuCl₃ layer intercalated into a single 5×5 graphene layer with the same stacking type. Both unstrained and strained structures are relaxed by keeping the strong C-C bond in graphene fixed while the α -RuCl₃ layer is fully relaxed.

We compute the electronic properties of both type of structures within DFT and compare them with those of pristine single-layer graphene and bulk α -RuCl₃. By aligning the electronic bands of the unstrained C-RuCl₃ with those of the pristine materials, we observe no significant hybridization between the graphene and α -RuCl₃ layers; instead, mostly charge transfer takes place (see Supplementary Material), in agreement with previous studies on similar heterostructures [12, 13, 34, 35]. Because the hybridization is effectively very weak, the applied strain in the simplified unit cell impacts only the α -RuCl₃ electronic structure, leaving the graphene bands unchanged except for a band shift due to charge transfer (see below). Using the graphene- α -RuCl₃ separation $d_{\text{Gr-RuCl}_3}$ suggested by X-ray data, we

find nearly identical charge depletion in both, strained and unstrained systems. We also tested different relative orientations and found that they produce no significant changes in the charge transfer (see Supplementary Material).

Based on (i) the absence of strong hybridization between the graphene and α -RuCl₃ layers, (ii) the fact that strain in the α -RuCl₃ layer does not appreciably modify the charge transfer, and (iii) the charge transfer is rather insensitive to the relative orientation of the layers, we conclude that the electronic graphene bands can be reliably obtained using a reduced unit cell with a tensile-strained α -RuCl₃ layer.

Following this approach, we model the experimental structures determined by XRD by constructing four geometries containing a tensile-strained 2×2 α -RuCl₃ layer intercalated with a 5×5 graphene supercell in the stacking arrangements A|A, AB|AB, ABAB|ABAB and ABCA|ABCA as shown in Figure 1. The theoretical structures AB|AB correspond to the S2 sample, and ABAB|ABAB and ABCA|ABCA to the S4 sample. Here, to reduce computational expense, we replicate the graphene stacking sequence after each α -RuCl₃ layer, simplifying the original stacking from A|AB|B to AB|AB, and AB|BCAB|BC (AB|BABA|AB) to ABCA|ABCA (ABAB|ABAB). This simplification is justified because the charge transfer is insensitive to the relative orientation between α -RuCl₃ and graphene, and the graphene sections are well separated by the intervening α -RuCl₃ layer. Our Bader analysis of the charge redistribution (Figure 3)

shows that the graphene sheets donate charge to the α - RuCl_3 sheet, and the charge mostly accumulates at the interface (Figure 3a). Furthermore, the total charge accumulated on the α - RuCl_3 layer increases with the number of intercalated graphene layers (see Supplementary Material for details). A similar trend has recently been reported in multilayer graphene heterostructures [36]. The magnitude of the charge accumulation is consistent with previous studies of related α - RuCl_3 /graphene systems [12, 19, 35]. When comparing the charge transfer between the different ABAB|ABAB and ABCA|ABCA stacking configurations, we find no significant differences.

In Figure 3b, we present the planar-averaged charge density along the c direction. In the A|A intercalation, every graphene layer exhibits the same charge depletion because of the periodicity of the unit cell. This also holds for the AB|AB intercalation, as each layer faces a α - RuCl_3 surface. In contrast, for the ABAB|ABAB or ABCA|ABCA configurations, charge depletion is concentrated primarily on the interface graphene layers, while the inner graphene layers remain screened.

Electronic properties

To understand the origin of the measured quantum oscillations, we estimate the corresponding frequencies using the Onsager relation [37], $F = \frac{\hbar}{2\pi e} S$, which links the frequencies F to the extremal Fermi surface cross-sectional area S . These are compared with the experimental data in Figure 2g and h. Since the magnetic field in the experiments is applied along the crystal c -axis, we consider Fermi surface cross sections perpendicular to k_z . Electronic structures and corresponding Fermi surfaces are calculated for each intercalated crystal.

The charge redistribution at the interface between α - RuCl_3 and the adjacent graphene layer is mostly localized at the Cl atoms as shown in Figure 3a with α - RuCl_3 remaining rather insulating [38]. Therefore, only the graphene layers are expected to contribute to the observed quantum oscillations. We compute the graphene layers electronic properties directly from the intercalated structures using non-spin-polarized GGA. The band structures are unfolded and projected onto graphene states, then compared to pristine, undoped graphene (Figure 4). Note the formation of a flat band with the number of stacked graphene layers, as has been observed in rhombohedral graphene stacking [4, 39–42]. In all intercalated cases, charge transfer induces hole pockets around the \mathbf{K} points.

In the A|A (Figure 4a) and AB|AB (Figure 4b) intercalations, the pristine graphene bands are preserved with a global Fermi energy shift of 0.68 eV and 0.48 eV, respectively, due to equivalent hole doping of the graphene layers (Figure 3b). The smaller shift in the bilayer AB|AB case arises because the transferred charge is distributed

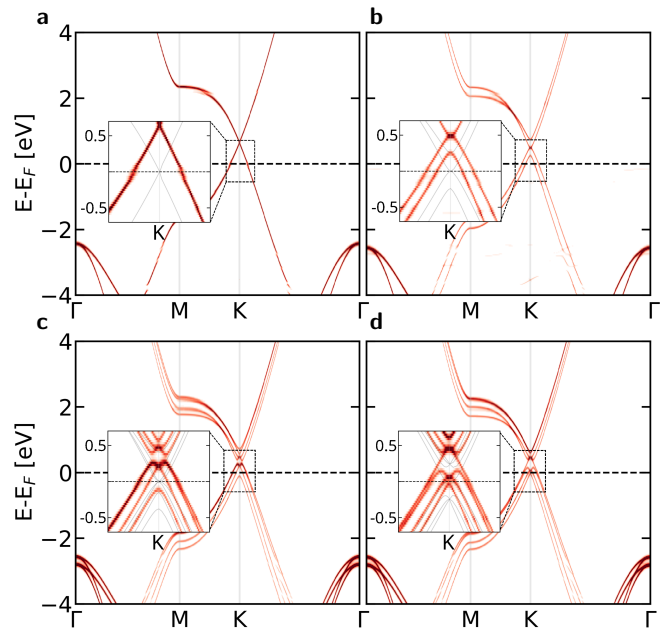


Figure 4. Unfolded electronic band structure of the C- RuCl_3 graphene layers in red for the four different intercalated geometries obtained via non-spin polarized GGA calculation, **a** A|A, **b** AB|AB, **c** ABAB|ABAB, and **d** ABCA|ABCA stacking. Each inner panel shows a zoomed region around the \mathbf{K} point. Light gray solid lines display the bands of pristine (multi-layered) graphene.

across two bands, whereas in the single-layer A|A case only one band contributes to the depletion. In the four-layer ABAB|ABAB and ABCA|ABCA stackings, the energy shift is non-uniform, reflecting the layer-dependent charge redistribution (Figure 4c, d). The pristine four-layer structures show four energy-separated bands, in agreement with previous studies [4, 39–42], while in the intercalated systems, two of these bands overlap or nearly overlap due to doping. The band geometry around \mathbf{K} also depends on the stacking, directly influencing the Fermi surface.

The Fermi surfaces are computed by unfolding the bands and projecting onto graphene states, focusing on the region around \mathbf{K} where the bands cross the Fermi level (Figure 5). The A|A intercalation yields a single hole pocket, consistent with prior experimental observations [10]. AB|AB produces two pockets of different sizes, while ABAB|ABAB and ABCA|ABCA exhibit three hole pockets. In the ABAB|ABAB, the three pockets are distinct, with the two outer bands overlapping, forming a larger pocket plus a smaller one. In the ABCA|ABCA, the three pockets are distinct, with the two outer bands nearly overlapping. Thus, the stacking sequence controls the number and size of Fermi hole pockets. We compute their areas and the corresponding quantum oscillation frequencies using the Onsager equation, and compare the calculated quantum oscillation frequencies with the experimentally measured ones ($\alpha \approx 91$ T,

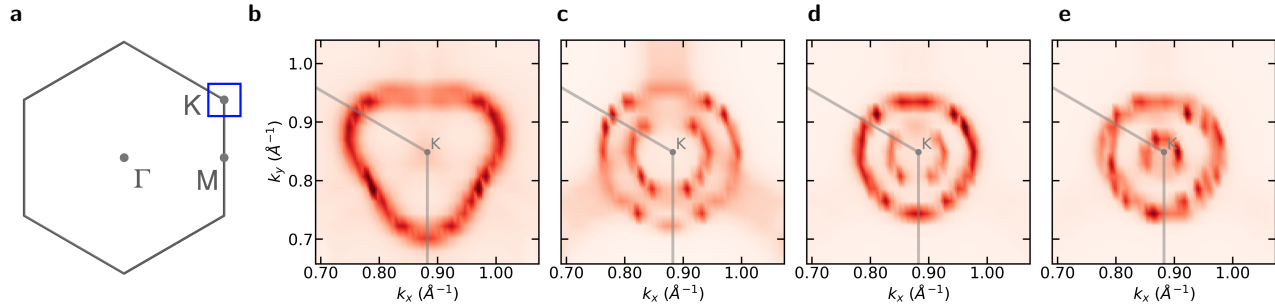


Figure 5. Unfolded Fermi surface of the graphene layers C-RuCl₃ structure calculated via a non-spin polarized GGA calculation. **a** Full Brillouin zone. The blue region indicates the calculated unfolded region around the K point. **b-e** Fermi surfaces for **b** A|A, **c** AB|AB, **d** ABAB|ABAB, and **e** ABCA|ABCA stackings.

$\beta \approx 170 - 176$ T).

Single-layer A|A intercalation produces a single high-frequency pocket (≈ 511 T), inconsistent with both quantum oscillations experiments and XRD, discarding this as the stacking pattern. AB|AB (S2-like) yields two pockets (131 T, 444 T), while four-layer ABAB|ABAB and ABCA|ABCA (S4-like) produce two and three pockets (70T, 296 T, and 28T, 311 T, 330 T), respectively. Although the agreement improves, discrepancies with the experiment remain. Examining their possible origin, we find that the Fermi-surface areas are highly sensitive to the interlayer distances ($d_{\text{Gr-Gr}}$, $d_{\text{Gr-RuCl}_3}$) and the amount of charge transfer. Modest Fermi-level shifts (≈ 0.1 eV) – consistent with plausible variations in interlayer spacing arising from, for example, stacking faults not included in our calculations – bring the computed frequencies into good agreement with experiment. A Fermi level shift of 0.1 eV yields two frequencies of 27 T and 183 T for the ABAB|ABAB stacking, and 126 T and 214 T for the ABCA|ABCA stacking. Further slight Fermi level shifts push the inner hole pocket below the Fermi energy, in which case no corresponding quantum oscillations can be observed. This behavior is consistent with the sample-dependent absence of the α frequency in the quantum oscillations measurements.

From this theoretical analysis, we conclude that the quantum oscillations response is governed by the stacking sequence, charge distribution, and structural variability. Stacking-fault effects further influence the observations but remain beyond our current computational resolution.

CONCLUSIONS

In summary, we have successfully synthesized graphite intercalated with α -RuCl₃ for the first time. By performing X-ray diffraction experiments we determined the crystal structure and showed that several different stackings can be achieved during the growth process. To characterize the properties of the system further, we performed transport experiments and Shubnikov–de Haas (SdH) quantum oscillations measurements. Compared to pristine graphite, which exhibits

only small SdH frequencies, the intercalated samples exhibit much higher frequencies of approximately 91T and 170 T, indicating substantial modifications of the Fermi surface.

Examining the different stackings identified by the XRD experiments by carrying out DFT calculations we find no strong hybridization between the graphite and α -RuCl₃ layers. Instead, our theoretical results reveal significant charge transfer from the graphite layers to the α -RuCl₃ layers which can be controlled by modifying the number of intercalated graphite layers between successive α -RuCl₃ sheets. The intercalation-dependent charge transfer strongly influences both the electronic band structure and Fermi surface of the crystal. These changes lead to a modified Fermi surface, consistent with the experimental SdH frequencies.

Our results show a promising first step of the realization of 3D structures that combine the flat-band, strongly correlated and topologically non-trivial physics of rhombohedral graphene with the unconventional magnetism, charge-transfer, and interfacial phenomena of graphene/ α -RuCl₃ heterostructures, opening a route to engineered bulk phases with exotic electronic, magnetic and topological behavior.

METHODS

Structure analysis:

We conducted XRD experiments for single crystal (nearly single crystal) samples in BL10XU/SPring-8 (X-ray wavelength: 0.4304 Å, X-ray beam size: 20 μm in diameter) and powder samples using an X-ray diffractometer (Bruker D2 Phaser) at the Institute for Advanced Materials and Manufacturing at UTK (X-ray wavelength 1.542 Å (Cu-K α)). We collected the XRD from a single crystal in a forward-scattering geometry with a 2-dimensional area detector (Varex Imaging XRD1611 CP3 Flat panel detector) while oscillating the sample ± 20 deg. XRD of the powder was challenging because grinding in a mortar could not crush the samples into fine powder. Therefore, we gathered many single crystals in the sample holder of the diffractometer to produce a powder-like condition. Thus, the obtained powder XRD is highly oriented. The typical

sample	a [Å]	c [Å]	Stacking
stage 2	29.62(3)	25.4(2)	A AB B
stage 4	29.5(4)	58.2(1)	AB BCAB BC or AB BABA AB

TABLE I. Experimentally obtained lattice constants for c -RuCl₃ and the suggested stacking of layers. The vertical line | indicates the α -CuCl₃ layer.

XRD images for the S2 and S4 single-crystal samples are in Figures S1c and d in the supplemental material. The XRD patterns for powder samples are in Figures S1a and b in the supplemental material.

First, we index the powder XRD peaks with hkl ($h = k = 0$) and the calculated lattice constant c are 25.4 Å for the S2 and 58.2 Å for the S4 samples, respectively. Those values are much larger than the typical values 6.7 Å of pure graphite, suggesting intercalation by α -RuCl₃. We estimated the number of RuCl₃ layers and figured out the stacking sequence of the graphene and α -RuCl₃ layers in a unit cell based on the analogy with FeCl₃, CrCl₃, and AlCl₃, [28–30] We adopted the following assumptions.

1. RuCl₃ crystallizes in a solid composed of Cl₃Ru₂Cl₃ and is incommensurate with the graphite host.
2. The graphene and RuCl₃ layers form a supercell constructed by combining $n \times m$ unit cells of RuCl₃ and $N \times M$ of graphene. Here, n , m , N , and M are integers.
3. The inter-layer distance between adjacent graphenes is about 3.5 ~ 4 Å, and the distance between two graphene layers that sandwich a RuCl₃ layer is about 9 ~ 10 Å.
4. Two adjacent graphene layers are stacked as AB, AC, or BC (Natural graphite has ABAB or ABCABC stacking). Two graphene layers that sandwich RuCl₃ in between stack AA, BB, or CC (all three are equivalent).

Figures S1a and b in the supplemental material show the hkl indexing for the single crystal samples. Note that all the observed peaks are for hkl ($l=0$) due to the large c -axis and limited sample oscillation angle during the XRD measurements. Based on the indexing results for powder and single crystal samples and the assumptions mentioned above, we conclude the crystal structure for the sample as shown in the Table I and Figure 1b, c and d.

Quantum Oscillations:

Magnetotransport experiments were performed in a physical property measurement system (PPMS-Quantum Design) under magnetic fields up to 9 T and temperatures as low as 1.8 K using a conventional four-terminal method. The

measurement was performed by passing the current in the ab -plane and applying the magnetic field along the c -axis of the crystal. The measured longitudinal and transverse resistivities were field-symmetrized and antisymmetrized, respectively, to correct the effect of contact misalignment.

Computational details:

We perform density functional theory (DFT) calculations as implemented in VASP [43] simulation package version 6.3.0. In all calculations we apply the Generalized Gradient Approximation (GGA) [44] as exchange-correlation functional. We use the following pseudopotentials in the projector augmented wave method (PAW) [45, 46] Ru_pv, Cl and C provided by the VASP package. In all calculations the basis set plane-wave cut-off for the expansion is set to 500 eV. In all crystal structures we relax the α -RuCl₃ layer and keep the graphene layers geometry fixed. The graphene- α -RuCl₃ layer distance is kept fixed at approximately the average experimental value of $d_{\text{Gr-RuCl}_3} = 3.60$ Å, the adjacent graphene sheets at $d_{\text{Gr-Gr}} = 3.54$ Å, and the C-C distance in each graphene layer is ≈ 1.42 Å, consistent with previous reports [47]. The relaxations are performed via the Γ -point version of VASP with a convergence criterion of the forces for each atom in the α -RuCl₃ layer in each direction of 0.005 eV/Å assuming a non-magnetic state. For the crystal cell optimization we include van der Waals corrections via the DFT-D3 method of Grimme [48, 49].

Further electronic properties are calculated on a $6 \times 6 \times 2$ k-mesh. The supercell electronic band structures are unfolded into the primitive Brillouin zone (BZ) by using the KPROJ software [50]. The Fermi surfaces are generated from sequences of unfolded electron band structures. The charge transfer was estimated via the Bader analysis [51], and k-mesh convergence has been checked. The spatial resolved charge transfer was calculated via the VASPKIT package [52]. The quantum oscillation frequencies are calculated from the unfolded graphene layers Fermi surfaces. Due to the smeared Fermi surfaces as a consequence of the unfolding, the Fermi pocket boundaries are taken from the highest intensity points and connected to form a closed area. Therefore, all reported frequencies inherit a small systematic error which does not change the conclusions of the study.

Additionally, as a cross-check we compute the quantum frequencies for the A|A structure via the C++ program dhva [53, 54], which implements the dHvA frequency extraction algorithm introduced by Rourke and Julian [55]. Calculations are performed on a supercell grid comprising 6.4×10^7 k-points distributed over 64 unit cells. Higher k-point density is obtained through tricubic interpolation [56]. The magnetic field is applied in the (001) direction.

Acknowledgements

A.R and R.V. thank the Deutsche Forschungsgemeinschaft

(DFG, German Research Foundation) for funding through the TRR 288 - 422213477 (project A05, B05) and gratefully acknowledge the computing time provided to them on the Goethe-HLR cluster at the Frankfurt Center for Scientific Computing. A.R. thanks Daniel Guterding for support of the hdva code (Github). S. M. and D. M. acknowledge the support from the Gordon and Betty Moore Foundation's EPiQS initiative, Grant GBMF9069 and the support from AFOSR MURI Grant No. FA9550-20-1-0322.

X-ray diffraction was performed at the Institute for Advanced Materials & Manufacturing (IAMM) Diffraction facility, located at the University of Tennessee, Knoxville, and at BL10XU/SPring-8 (Proposal number 2024B1285).

Author Contributions

N.H. and M.C synthesized the crystals. S.M. performed the transport and quantum oscillation measurements. T.M. and M.C. performed the X-ray experiments. A.R. performed the *ab initio* simulations. R.V. and D.M. conceived and supervised the project. All authors contributed to the discussions and writing of the manuscript.

Conflict of interest

The authors declare no conflict of interest.

Data availability statement

The datasets generated during the current study are available upon reasonable request. (not applicable)) The authors declare no conflict of interest.

-
- [1] S. C. de la Barrera, S. Aronson, Z. Zheng, K. Watanabe, T. Taniguchi, Q. Ma, P. Jarillo-Herrero, and R. Ashoori, Cascade of isospin phase transitions in bernal-stacked bilayer graphene at zero magnetic field, *Nature Physics* **18**, 771 (2022).
- [2] Z. Li, X. Kuang, A. Jimeno-Pozo, H. Sainz-Cruz, Z. Zhan, S. Yuan, and F. Guinea, Charge fluctuations, phonons, and superconductivity in multilayer graphene, *Physical Review B* **108**, 045404 (2023).
- [3] G. Wagner, Y. H. Kwan, N. Bultinck, S. H. Simon, and S. Parameswaran, Superconductivity from repulsive interactions in bernal-stacked bilayer graphene, *Physical Review B* **110**, 214517 (2024).
- [4] H. Henck, J. Avila, Z. Ben Aziza, D. Pierucci, J. Baima, B. Pamuk, J. Chaste, D. Utt, M. Bartos, K. Nogajewski, *et al.*, Flat electronic bands in long sequences of rhombohedral-stacked graphene, *Physical Review B* **97**, 245421 (2018).
- [5] J. Dong, T. Wang, T. Wang, T. Soejima, M. P. Zaletel, A. Vishwanath, and D. E. Parker, Anomalous hall crystals in rhombohedral multilayer graphene. i. interaction-driven chern bands and fractional quantum hall states at zero magnetic field, *Physical Review Letters* **133**, 206503 (2024).
- [6] B. A. Bernevig and Y. H. Kwan, "berry trashcan" model of interacting electrons in rhombohedral graphene, arXiv preprint arXiv:2503.09692 (2025).
- [7] W. Zhou, J. Ding, J. Hua, L. Zhang, K. Watanabe, T. Taniguchi, W. Zhu, and S. Xu, Layer-polarized ferromagnetism in rhombohedral multilayer graphene, *Nature Communications* **15**, 2597 (2024).
- [8] Y. Choi, Y. Choi, M. Valentini, C. L. Patterson, L. F. Holleis, O. I. Sheekey, H. Stoyanov, X. Cheng, T. Taniguchi, K. Watanabe, *et al.*, Superconductivity and quantized anomalous hall effect in rhombohedral graphene, *Nature*, 1 (2025).
- [9] T. Han, Z. Lu, Z. Hadjri, L. Shi, Z. Wu, W. Xu, Y. Yao, A. A. Cotten, O. Sharifi Sedeh, H. Weldeyesus, *et al.*, Signatures of chiral superconductivity in rhombohedral graphene, *Nature* **643**, 654 (2025).
- [10] S. Mashhadi, Y. Kim, J. Kim, D. Weber, T. Taniguchi, K. Watanabe, N. Park, B. Lotsch, J. H. Smet, M. Burghard, *et al.*, Spin-split band hybridization in graphene proximitized with α -rucl₃ nanosheets, *Nano letters* **19**, 4659 (2019).
- [11] B. Zhou, J. Balgley, P. Lampen-Kelley, J.-Q. Yan, D. G. Mandrus, and E. A. Henriksen, Evidence for charge transfer and proximate magnetism in graphene- α -rucl₃ heterostructures, *Physical Review B* **100**, 165426 (2019).
- [12] S. Biswas, Y. Li, S. M. Winter, J. Knolle, and R. Valentí, Electronic properties of α -rucl₃ in proximity to graphene, *Phys. Rev. Lett.* **123**, 237201 (2019).
- [13] V. Leeb, K. Polyudov, S. Mashhadi, S. Biswas, R. Valentí, M. Burghard, and J. Knolle, Anomalous quantum oscillations in a heterostructure of graphene on a proximate quantum spin liquid, *Physical Review Letters* **126**, 097201 (2021).
- [14] D. J. Rizzo, B. S. Jessen, Z. Sun, F. L. Ruta, J. Zhang, J.-Q. Yan, L. Xian, A. S. McLeod, M. E. Berkowitz, K. Watanabe, *et al.*, Charge-transfer plasmon polaritons at graphene/ α -rucl₃ interfaces, *Nano letters* **20**, 8438 (2020).
- [15] A. Banerjee, C. Bridges, J.-Q. Yan, A. Aczel, L. Li, M. Stone, G. Granroth, M. Lumsden, Y. Yiu, J. Knolle, *et al.*, Proximate kitaev quantum spin liquid behaviour in a honeycomb magnet, *Nature materials* **15**, 733 (2016).
- [16] S. M. Winter, K. Riedl, P. A. Maksimov, A. L. Chernyshev, A. Honecker, and R. Valentí, Breakdown of magnons in a strongly spin-orbital coupled magnet, *Nature communications* **8**, 1152 (2017).
- [17] S. M. Winter, A. A. Tsirlin, M. Daghofer, J. van den Brink, Y. Singh, P. Gegenwart, and R. Valentí, Models and materials for generalized kitaev magnetism, *Journal of Physics: Condensed Matter* **29**, 493002 (2017).
- [18] S. Trebst and C. Hickey, Kitaev materials, *Physics Reports* **950**, 1 (2022).
- [19] J. Balgley, J. Butler, S. Biswas, Z. Ge, S. Lagasse, T. Taniguchi, K. Watanabe, M. Cothrine, D. G. Mandrus, J. Velasco Jr, *et al.*, Ultrasharp lateral p-n junctions in modulation-doped graphene, *Nano Letters* **22**, 4124 (2022).
- [20] C. Ojeda-Aristizabal, X. Zheng, C. Xu, Z. Nussinov, Y. Motome, A. Banerjee, A. W. Tsen, M. Knap, R.-R. Du, G. Joshi, *et al.*, Lessons from α -rucl₃ for pursuing quan-

- tum spin liquid physics in atomically thin materials, arXiv preprint arXiv:2511.13838 (2025).
- [21] M. S. Dresselhaus and G. Dresselhaus, Intercalation compounds of graphite, *Advances in Physics* **30**, 139 (1981).
- [22] A. Chernyshev and O. Starykh, Roller coaster in a flatland: Magnetoresistivity in eu-intercalated graphite, *Physical Review X* **12**, 021010 (2022).
- [23] R. Hui, F.-Y. Kang, Q.-J. Jiao, and W.-C. Shen, Synthesis criterion for a metal chloride-graphite intercalation compound by a molten salt method, *New carbon materials* **24**, 18 (2009).
- [24] R. Matsumoto and Y. Okabe, Electrical conductivity and air stability of FeCl_3 , CuCl_2 , MoCl_5 , and SbCl_5 graphite intercalation compounds prepared from flexible graphite sheets, *Synthetic Metals* **212**, 62 (2016).
- [25] S. Flandrois, J.-M. Masson, J.-C. Rouillon, J. Gaultier, and C. Hauw, Intercalation compounds of graphite with nickel chloride: synthesis, structure, and mechanism of intercalation, *Synthetic Metals* **3**, 1 (1981).
- [26] S.-S. Tzeng, P.-L. Wang, and T.-H. Ko, Effects of processing parameters on the structure and amount of intercalation of copper chloride-graphite intercalation compounds, *Journal of materials science* **36**, 497 (2001).
- [27] V. Postnikov, A. Zvarykina, Y. V. Salyn', Y. T. Struchkov, Y. N. Novikov, and M. Vol'pin, Synthesis and structure of layer-type graphite compounds with ruthenium, palladium, and osmium chlorides, *Journal of Structural Chemistry* **18**, 819 (1977).
- [28] M. S. Dresselhaus and G. Dresselhaus, Intercalation compounds of graphite, *Advances in Physics* **51**, 1 (2002).
- [29] J. M. Cowley and J. A. Ibers, The structures of some ferric chloride-graphite compounds, *Acta Crystallographica* **9**, 421 (1956).
- [30] E. Stumpp, The intercalation of metal chlorides and bromides into graphite, *Materials Science and Engineering* **31**, 53 (1977).
- [31] B. Camargo, Y. Kopelevich, A. Usher, and S. Hubbard, Effect of structural disorder on quantum oscillations in graphite, *Applied Physics Letters* **108** (2016).
- [32] R. de Jesus, B. Camargo, R. da Silva, Y. Kopelevich, M. Behar, M. Gusmão, and P. Pureur, Magneto-transport properties of as-implanted highly oriented pyrolytic graphite, *Physica B: Condensed Matter* **500**, 118 (2016).
- [33] K. Momma and F. Izumi, *VESTA3* for three-dimensional visualization of crystal, volumetric and morphology data, *Journal of Applied Crystallography* **44**, 1272 (2011).
- [34] A. Rossi, C. Johnson, J. Balgley, J. C. Thomas, L. Francaviglia, R. Dettori, A. K. Schmid, K. Watanabe, T. Taniguchi, M. Cothrine, *et al.*, Direct visualization of the charge transfer in a graphene/ α - rUCl_3 heterostructure via angle-resolved photoemission spectroscopy, *Nano Letters* **23**, 8000 (2023).
- [35] A. Razpopov and R. Valentí, Ab initio study of highly tunable charge transfer in β - rUCl_3 /graphene heterostructures, *Physical Review Research* **6**, 043026 (2024).
- [36] F. Falorsi, S. Zhao, K. Liu, C. Eckel, J. F. Pöhls, W. Bennecke, M. Reutzler, S. Mathias, K. Watanabe, T. Taniguchi, *et al.*, Interlayer charge transfer in graphene-2d polyimide heterostructures, *2D Materials* **12**, 025011 (2025).
- [37] L. Onsager, Interpretation of the de Haas-van Alphen effect, *The London, Edinburgh, and Dublin Philosophical Magazine and Journal of Science* **43**, 1006 (1952).
- [38] X. Zheng, Z.-X. Liu, C. Zhang, H. Zhou, C. Yang, Y. Shi, K. Tanigaki, and R.-R. Du, Incommensurate charge supermodulation and hidden dipole order in layered kitaev material α - rUCl_3 , *Nature Communications* **15**, 7658 (2024).
- [39] M. Aoki and H. Amawashi, Dependence of band structures on stacking and field in layered graphene, *Solid State Communications* **142**, 123 (2007).
- [40] L. I. Johansson, R. Armiento, J. Avila, C. Xia, S. Lorcy, I. A. Abrikosov, M. C. Asensio, and C. Virojanadara, Multiple π -bands and bernal stacking of multilayer graphene on c-face SiC, revealed by nano-angle resolved photoemission, *Scientific Reports* **4**, 4157 (2014).
- [41] R. Yagi, T. Hirahara, R. Ebisuoka, T. Nakasuga, S. Tajima, K. Watanabe, and T. Taniguchi, Low-energy band structure and even-odd layer number effect in ab-stacked multilayer graphene, *Scientific Reports* **8**, 13018 (2018).
- [42] Y. Zhang, Y.-Y. Zhou, S. Zhang, H. Cai, L.-H. Tong, W.-Y. Liao, R.-J. Zou, S.-M. Xue, Y. Tian, T. Chen, *et al.*, Layer-dependent evolution of electronic structures and correlations in rhombohedral multilayer graphene, *Nature Nanotechnology* **20**, 222 (2025).
- [43] G. Kresse and J. Hafner, Ab initio molecular dynamics for liquid metals, *Phys. Rev. B* **47**, 558 (1993).
- [44] J. P. Perdew, K. Burke, and M. Ernzerhof, Generalized gradient approximation made simple [phys. rev. lett. 77, 3865 (1996)], *Phys. Rev. Lett.* **78**, 1396 (1997).
- [45] P. E. Blöchl, Projector augmented-wave method, *Physical Review B* **50**, 17953 (1994), publisher: American Physical Society.
- [46] G. Kresse and D. Joubert, From ultrasoft pseudopotentials to the projector augmented-wave method, *Physical Review B* **59**, 1758 (1999), publisher: American Physical Society.
- [47] D.-M. Chen, P. M. Shenai, and Y. Zhao, Tight binding description on the band gap opening of pyrene-dispersed graphene, *Phys. Chem. Chem. Phys.* **13**, 1515 (2011).
- [48] S. Grimme, J. Antony, S. Ehrlich, and H. Krieg, A consistent and accurate ab initio parametrization of density functional dispersion correction (dft-d) for the 94 elements h-pu, *The Journal of chemical physics* **132** (2010).
- [49] S. Grimme, S. Ehrlich, and L. Goerigk, Effect of the damping function in dispersion corrected density functional theory, *Journal of computational chemistry* **32**, 1456 (2011).
- [50] J. Chen, M. Weinert, and M. Chen, Kproj: A program for unfolding electronic and phononic bands, *Computer Physics Communications* **312**, 109614 (2025).
- [51] G. Henkelman, A. Arnaldsson, and H. Jónsson, A fast and robust algorithm for bader decomposition of charge density, *Computational Materials Science* **36**, 354 (2006).
- [52] V. Wang, N. Xu, J.-C. Liu, G. Tang, and W.-T. Geng, Vaspkit: A user-friendly interface facilitating high-throughput computing and analysis using vasp code, *Computer Physics Communications* **267**, 108033 (2021).
- [53] S. Backes, D. Guterding, H. O. Jeschke, and R. Valentí, Electronic structure and de Haas-van Alphen frequencies in kFe_2As_2 within $\text{LDA} + \text{DMFT}$, *New Journal of Physics* **16**, 083025 (2014).
- [54] D. Guterding, *dhva: a code for calculating de haas-van*

[alphen frequencies and electronic band masses](#) (2014), accessed: 2025-03-01.

- [55] S. Julian, Numerical extraction of de haas–van alphen frequencies from calculated band energies, *Computer Physics Communications* **183**, 324 (2012).
- [56] F. Lekien and J. Marsden, Tricubic interpolation in three dimensions, *International Journal for Numerical Methods in Engineering* **63**, 455 (2005).

α -RuCl₃ intercalated into graphite: a new three-dimensional platform for exotic quantum phases - Supplementary Information -

Aleksandar Razpopov,^{1,*} Shirin Mozaffari,^{2,3,†} Takahiro Matsuoka,^{2,4,‡}
Matthew Cothrine,² Nan Huang,² Roser Valentí,^{1,§} and David Mandrus^{2,¶}

¹*Institut für Theoretische Physik, Goethe-Universität, 60438 Frankfurt am Main, Germany*

²*Department of Materials Sciences and Engineering,
The University of Tennessee, Knoxville, TN 37996, USA*

³*Department of Physics and Astronomy, Clemson University, Clemson, SC 29634, USA*

⁴*National Institute of Physics, University of the Philippines Diliman, Quezon, Metro Manila 1101, Philippines*

X-RAY DIFFRACTION ANALYSIS

In Figure S1 we show the XRD images and the integrated XRD profiles for stage 2 and stage 4 C-RuCl₃ samples.

SUPERCELLS CALCULATIONS WITH DIFFERENT ORIENTATIONS

We analyze the influence of relative orientation between the α -RuCl₃ and the Graphene layers on the charge transfer. Therefore, we calculate the electron properties of one intercalated $5 \times 5 \times 1$ α -RuCl₃ layer sandwiched between single $12 \times 12 \times 1$ Graphene layers alternating in the crystallographic c-direction, as shown in Figure S2a.

We consider two different relative orientations A and B, see Figure S2b. In both initial geometries the graphene-graphene layer distance ($d_{\text{Gr-Gr}}$) is 10.241 Å and the distance between the α -RuCl₃ and the graphene layer ($d_{\text{Gr-RuCl}_3}$) is 3.765 Å. The C-C distance ($d_{\text{C-C}}$) within the graphene layer is 1.434 Å, the Ru-Ru distance in the α -RuCl₃ layer is 3.443/3.441 Å. This corresponds to a tensile strain of $\approx 1\%$ compared to the relaxed C2/m structure of α -RuCl₃ [1]. The structures are fully optimized via non-spin polarized GGA calculation using the VASP package [2].

For the relaxed structures we calculate the non-spin polarized electronic band structures and density of states. The results for both orientations are shown in Figure S3. Due to a significant charge transfer from graphene to α -RuCl₃, the Dirac cone of graphene is shifted ≈ 0.7 eV above the Fermi surface. We note that due to the super-cell choice of the graphene layer, the K point is folded at the Γ -point, see Ref. [3]. This is more evident in the density of states, which vanishes at the Dirac cone, as highlighted in the zoomed-in energy range shown in the 3rd panel of Figure S3a for orientation A and Figure S3b for orientation B. The energy shift for both orientation is nearly identical which means that the charge transfer does not depend on the relative orientation. This results are comparable to the observation in Ref. [4, 5].

By unfolding the electronic band structure of the super cell, as shown in Figure S3, we clearly show the Dirac cone shift, see Figure S5a. The pristine Graphene bands (shown in Grey) reproduce by unfolded bands by a global band energy shifted of ≈ 0.7 eV. This indicates that there is a weak hybridization between the graphene and α -RuCl₃ layers but the charge transfer plays a significant role. In Figure S5b we display the unfolded α -RuCl₃ band structures obtained by non-spin polarized GGA simulation. The α -RuCl₃ bands do not show significant deviations from the pristine case. A zoomed-in region close to the Fermi energy shows a slight down shift of the bands, see Figure S5c.

CHARGE TRANSFER REDISTRIBUTION

Using Bader [6] analysis we analyze the charge transfer depletion and accumulation for different intercalated crystals. First, we analyze the charge transfer as function of the c lattice constant in the tensile single-layer stacking (A|A), and compare it to the non-tensile single-layer stacking crystal. We find that the charge transfer is strongly affected by the graphene layer- α -RuCl₃-distance $d_{\text{Gr-Ru}}$. At a distance $d_{\text{Gr-Ru}}$ which reassembles the distance in the unstrained structure, the charge transfer is almost identical, see Figure S4a. Next, we analyze the charge transfer as function of the intercalation stacking, results are summarized in Figure S4b. Our analysis shows that by increasing the number of the intercalated

* razpopov@itp.uni-frankfurt.de

† shirinm@clemson.edu

‡ tmatsuoka@up.edu.ph

§ valenti@itp.uni-frankfurt.de

¶ dmandrus@utk.edu

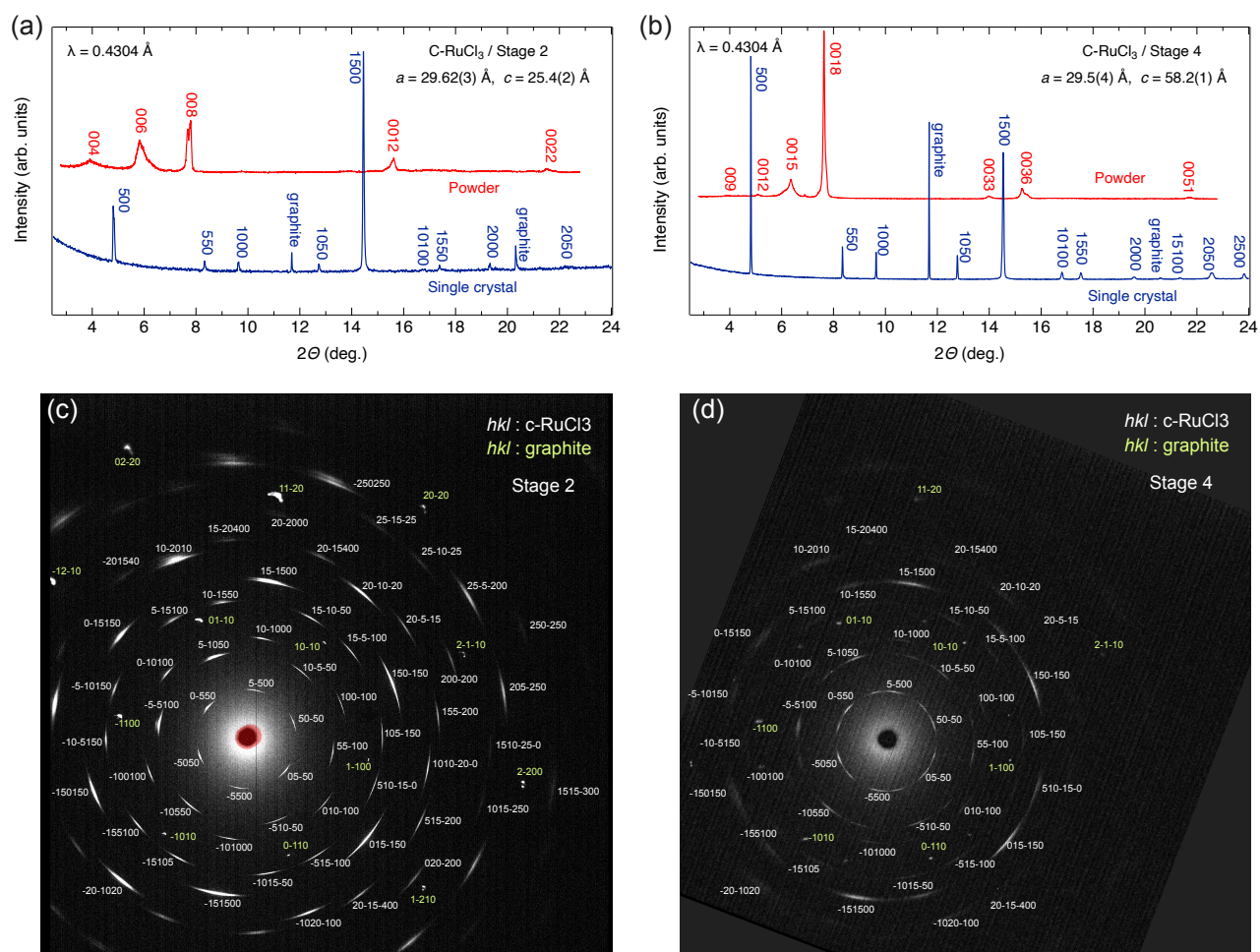


Figure S1: XRD images and the integrated XRD profiles for stage 2 and stage 4 C-RuCl₃ samples. **a** XRD images of the stage 2 (S2) single crystal and **b** the stage 4 (S4) single crystal samples. The *hkl* indices are shown together. **c** The integrated XRD profiles for S2 powder and single crystal samples, and **d** for S4 powder and single crystal samples. To compare the XRD profiles between the powder and single crystal samples, the powder-XRD data obtained using $\lambda = 1.541 \text{ \AA}$ x-ray are converted to the data for $\lambda = 0.4304 \text{ \AA}$. Note that the actual state of the single crystal samples is highly oriented polycrystalline, thus 'nearly single crystalline.' Due to the forward scattering geometry of the XRD instruments and the limited possible oscillation angles, the *hkl* ($l \neq 0$) reflections cannot be observed.

graphene layers the charge transfer increases significantly. A comparison of the charge accumulation in the ABAB|ABAB and ABCA|ABCA stacking configurations reveals only negligible differences, indicating that the relative stacking orientation plays a minor role in determining the charge transfer magnitude.

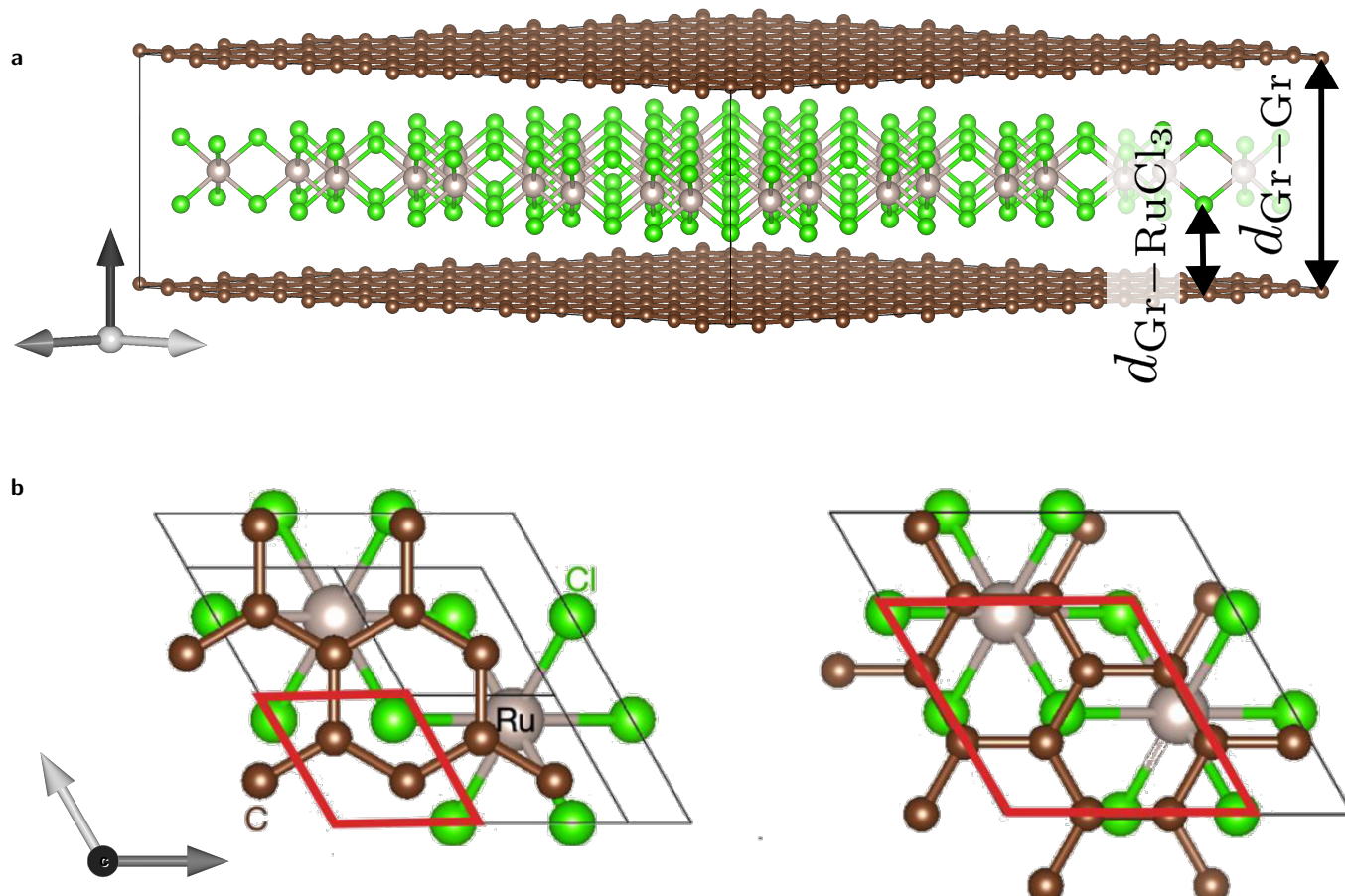


Figure S2: Bulk crystal structure of α - RuCl_3 intercalated in graphite. **a** side view showing the alternating graphene and α - RuCl_3 layers in the c -direction. **b** The two different relative orientations A and B considered in the study. On the left is the orientation A and on the right the orientation B structure.

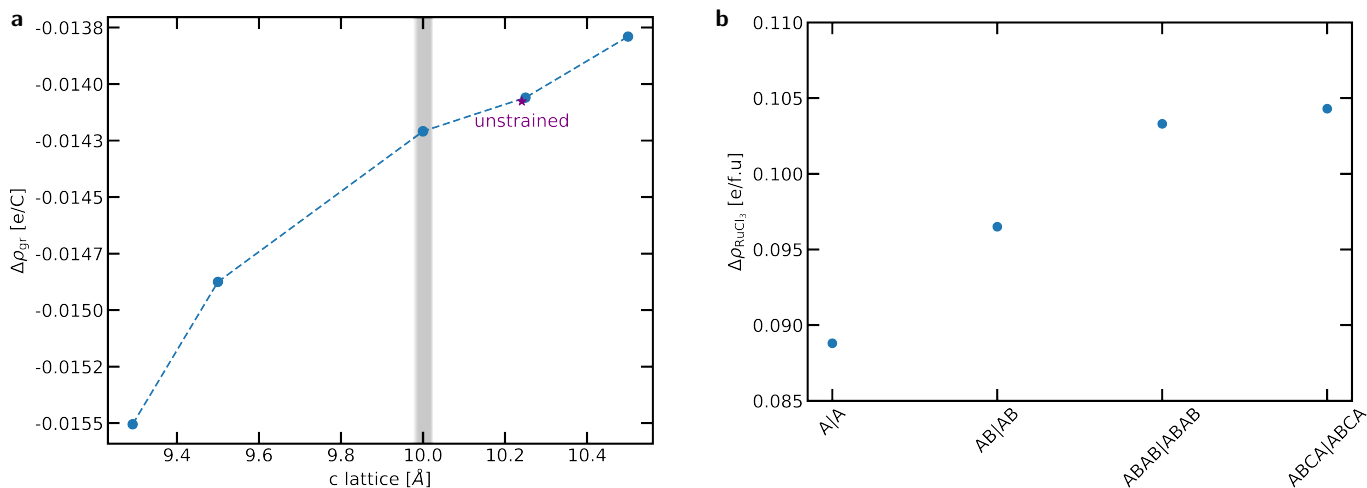


Figure S4: **a** shows the calculated charge transfer in the Gr layer as function of the c lattice constant in the tensile strained single-layer intercalation stacking (A|A). The purple data points presents the unstrained single-layer stacking structure. In the gray shaded area the $d_{\text{Gr-Ru}}$ of the strained and unstrained crystals are almost identical. Please note, the dashed lines between the data points are only an eye guide. **b** Calculated charge transfer on the α - RuCl_3 layer for each intercalation, A|A, AB|AB, ABAB|ABAB, and ABCA|ABCA. Positive sign refers to charge accumulation and negative to charge depletion.

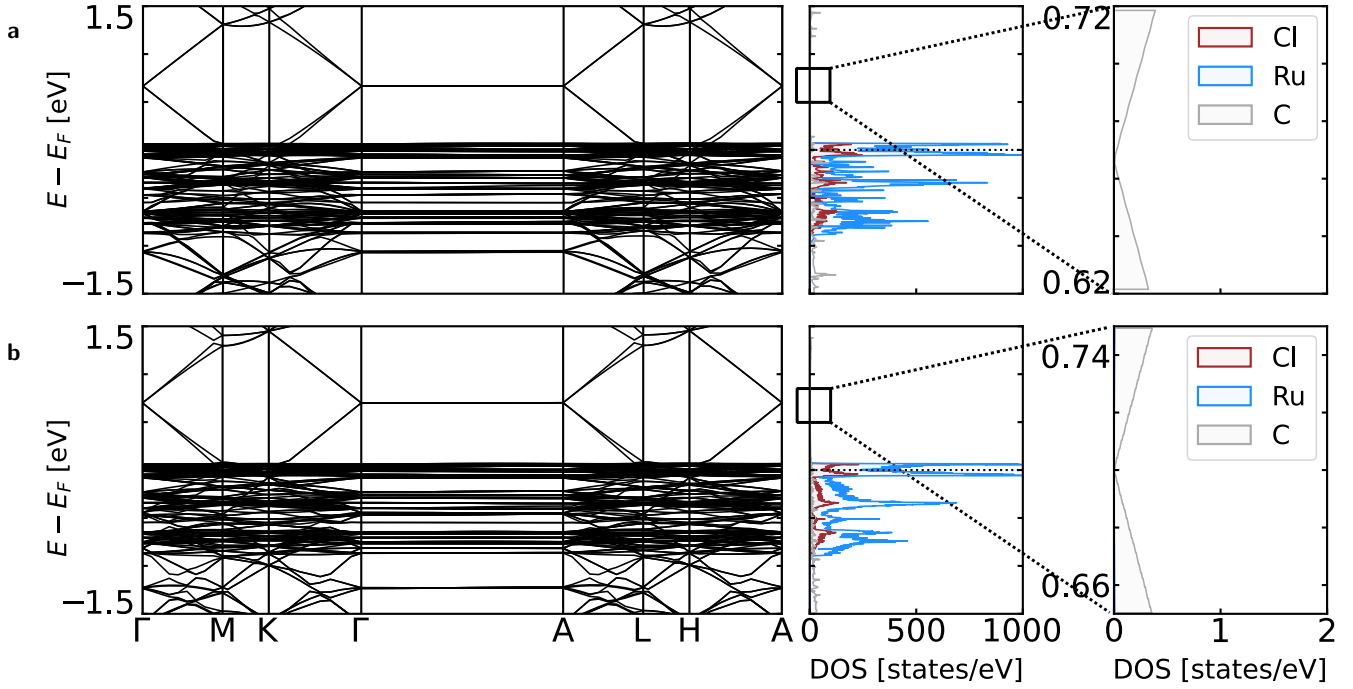


Figure S3: Calculated electronic band structure and atom-resolved density of states (DOS) within GGA for the relative orientations **a** A and **b** B. The 3rd panel is a blow-up of the shifted Dirac cone of graphene due to the charge transfer between graphene and α -RuCl₃.

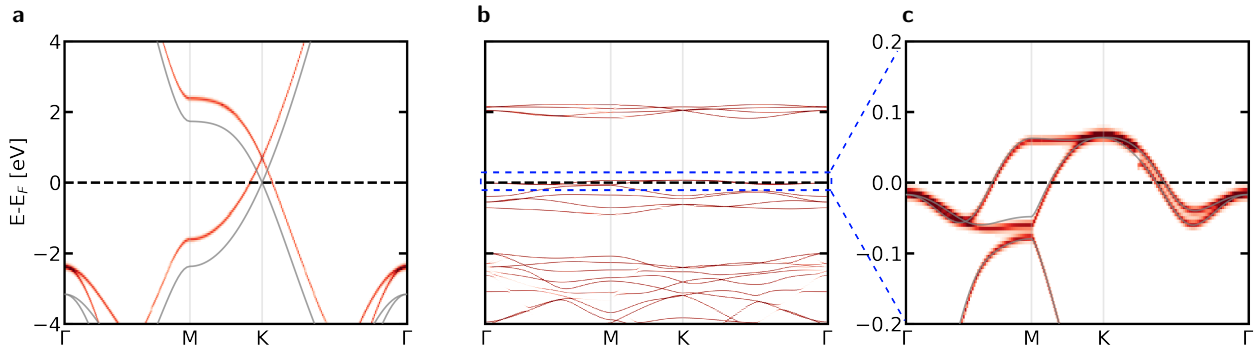


Figure S5: Unfolded band structure of zero-strain α -RuCl₃ layer intercalated with single layer Graphene layers obtained via non-spin polarized GGA calculation. The unit cell consists of 5×5 - α -RuCl₃ and 12×12 -Graphene. **a** shows the unfolded Graphene electronic bands. **b** shows the unfolded α -RuCl₃ electronic bands, and **c** shows a zoomed energy window around the Fermi energy of the α -RuCl₃ bands. The grey lines represent the electron bands of the pristine Graphene and α -RuCl₃ crystal structures.

-
- [1] B. Wolf, D. Kaib, A. Razpopov, S. Biswas, K. Riedl, S. Winter, R. Valentí, Y. Saito, S. Hartmann, E. Vinokurova, *et al.*, Combined experimental and theoretical study of hydrostatic he-gas pressure effects in α -rucl₃, *Physical Review B* **106**, 134432 (2022).
 - [2] G. Kresse and J. Hafner, Ab initio molecular dynamics for liquid metals, *Phys. Rev. B* **47**, 558 (1993).
 - [3] Y.-C. Zhou, H.-L. Zhang, and W.-Q. Deng, A 3n rule for the electronic properties of doped graphene, *Nanotechnology* **24**, 225705 (2013).
 - [4] S. Biswas, Y. Li, S. M. Winter, J. Knolle, and R. Valentí, Electronic properties of α -rucl₃ in proximity to graphene, *Phys. Rev. Lett.* **123**, 237201 (2019).
 - [5] A. Razpopov and R. Valentí, Ab initio study of highly tunable charge transfer in β -rucl₃/graphene heterostructures, *Physical Review Research* **6**, 043026 (2024).
 - [6] G. Henkelman, A. Arnaldsson, and H. Jónsson, A fast and robust algorithm for bader decomposition of charge density, *Computational Materials Science* **36**, 354 (2006).